Journal of Power Sources 192 (2009) 435–441

Contents lists available at ScienceDirect

Journal of Power Sources

journal homepage: www.elsevier.com/locate/jpowsour

Heat sources in proton exchange membrane (PEM) fuel cells

Julien Ramousse[a,*], Olivier Lottin[b], Sophie Didierjean[b], Denis Maillet[b]

[a] Laboratoire Optimisation de la Conception et Ingénierie de l'Environnement, FRE CNRS 3220, Université de Savoie, Campus scientifique, Savoie Technolac, 73376 Le Bourget du Lac - CEDEX, France
[b] Laboratoire d'Énergétique et de Mécanique Théorique et Appliquée, UMR 7563 CNRS–INPL–UHP, 2, avenue de la forêt de Haye, BP 160, 54504 Vandoeuvre lès Nancy CEDEX, France

ARTICLE INFO

Article history:
Received 30 January 2009
Received in revised form 16 March 2009
Accepted 18 March 2009
Available online 27 March 2009

Keywords:
Heat sources
Thermodynamic
Half-reaction entropy
Electrochemical activation
Joule effect
Water sorption enthalpy
Water condensation/evaporation

ABSTRACT

In order to model accurately heat transfer in PEM fuel cell, a particular attention had to be paid to the assessment of heat sources in the cell. Although the total amount of heat released is easily computed from its voltage, local heat sources quantification and localization are not simple. This paper is thus a discussion about heat sources/sinks distribution in a single cell, for which many bold assumptions are encountered in the literature. The heat sources or sinks under consideration are: (1) half-reactions entropy, (2) electrochemical activation, (3) water sorption/desorption at the GDL/membrane interfaces, (4) Joule effect in the membrane and (5) water phase change in the GDL.

A detailed thermodynamic study leads to the conclusion that the anodic half-reaction is exothermic ($\Delta S^{a}_{rev} = -226\,\mathrm{J\,mol^{-1}\,K^{-1}}$), instead of being athermic as supposed in most of the thermal studies. As a consequence, the cathodic half-reaction is endothermic ($\Delta S^{c}_{rev} = +62.8\,\mathrm{J\,mol^{-1}\,K^{-1}}$), which results in a heat sink at the cathode side, proportional to the current. In the same way, depending on the water flux through the membrane, sorption can create a large heat sink at one electrode and an equivalent heat source at the other. Water phase change in the GDL – condensation/evaporation – results in heat sources/sinks that should also be taken into account. All these issues are addressed in order to properly set the basis of heat transfer modeling in the cell.

1. Introduction

Thermal modeling is of great interest for improving hydrogen PEM fuel cell electrical performances. As highlighted in several publications [1–3], temperature effects on fuel cell voltage are not negligible. Actually, mass and charge transfers depend strongly on temperature. On the other hand, thermal transfer also depends on mass and charge transfer. Thus, pertinent thermal models constitute a key factor for understanding fuel cell electrical behaviour.

Comprehensive reviews of thermal management issues are presented by Faghri and Guo [4] and by Wang [5]. Since the first description of coupled heat and mass transfer proposed by Fuller and Newman [6], many similar works [7–9] have been published. All these studies allow to calculate temperature profiles through the membrane electrodes assembly (MEA) thickness.

Heat sources distribution and quantification determine the temperature profiles and they have to be properly estimated. The mechanisms responsible for heat production in PEM fuel cell MEA are complex, which makes it difficult to localize and quantify accurately all sources. For instance, Ju et al. [10] and Naterer et al. [11] paid a particular attention to the estimation of heat sources. Their models take into account the Joule effect, caused by the charge transfer resistances, the reversible heat of reaction and the irreversible heat production caused by the electrochemical reactions. However, the anodic half-reaction is assumed isothermal and water sorption/desorption phenomena are not taken into account, as in most of the models proposed in the literature. Such assumptions lead to inaccurate descriptions of heat transfer in the cell. A complete set of thermodynamical equations was established by Kjelstrup and Rosjorde [12] who evaluate the entropy production rate within the cell. However, the local values attributed to each phenomenon do not appear explicitly because of the global approach they used.

This paper focuses on heat sources modeling in PEMFC. The next section shows how the total amount of heat produced by the cell can be computed from its output voltage. Then, a detailed discussion about heat sources/sinks quantification and localization is given in order to properly distribute heat sources in the cell. The following phenomena are considered: half-reactions entropy, electrochemical activation, water sorption/desorption at the gas diffusion layer (GDL)/membrane interfaces, Joule effect in the membrane and water phase change in the GDL. Finally, the magnitudes of the heat sources are plotted as functions of the current density.

* Corresponding author. Tel.: +33 04 79 75 88 20; fax: +33 04 79 75 81 44.
E-mail address: julien.ramousse@univ-savoie.fr (J. Ramousse).

0378-7753/$ – see front matter © 2009 Elsevier B.V. All rights reserved.
doi:10.1016/j.jpowsour.2009.03.038

Nomenclature

a	activity
E	voltage (V)
e	elementary charge ($e = 1.6 \times 10^{-19}$ C)
F	Faraday's constant ($F = 96{,}485$ C)
RH	relative humidity
i	current density (A m^{-2})
L_m	membrane thickness (m)
N_{H_2O}	water flux (mol m^{-2} s^{-1})
N_A	Avogadro's number ($N_A = 6.02 \times 10^{23}$ mol^{-1})
P	pressure (Pa)
P_{sat}	saturation pressure (Pa)
Q	energy (J mol^{-1})
$\dot{Q}$	surfacic heat source (W m^{-2})
$\dot{q}$	volumic heat source (W m^{-3})
R_{ohm}	membrane resistance (Ω m^2)
r_{eff}	effective ionic radius (Å)
T	temperature (K)
W	electrical power density (W m^{-2})

Greek letters

ΔH	enthalpy (kJ mol^{-1})
ΔG	free Gibbs energy (kJ mol^{-1})
ΔS	entropy (J mol^{-1} K^{-1})
ε_0	absolute permittivity (F m^{-1})
ε_r	relative static permittivity (F m^{-1})
λ	water content
σ_{H^+}	protonic conductivity (S m^{-1})
η	activation overpotential (V)

Subscripts

e^-	electron
H^+	proton
H_2	hydrogen
H_2O	water
O_2	oxygen
ΔV	voltage losses
J	Joule
act	activation
reac	reaction
rev	reversible
irr	irreversible
sorp	sorption/desorption
c/e	condensation/evaporation
water	cooling water

Superscripts

°	standard conditions
a	anodic
c	cathodic
th	theoretical
tot	total

2. Total heat flux

Heat sources are directly related to voltage drops: the chemical energy supplied by the gases not converted into electricity is released as heat. Fig. 1 illustrates the links between heat production and voltage losses.

The chemical power supplied by the gases is a function of the enthalpy of the global reaction:

$$H_2 + 1/2O_2 \rightarrow H_2O \quad (1)$$

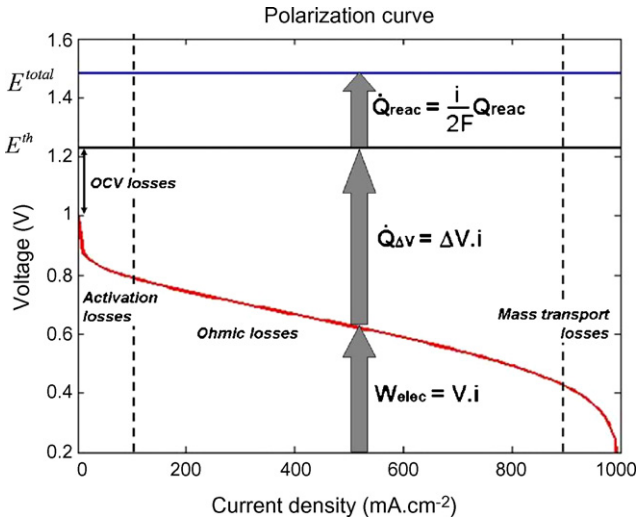

Fig. 1. Polarization curve and heat sources (standard conditions).

In standard conditions:

$$\Delta H^{tot}(T^0, P^0) = \Delta H^f_{H_2O} - \Delta H^f_{H_2} - 1/2\Delta H^f_{O_2} \quad (2)$$

From the reaction enthalpy $\Delta H^{tot}(T,P)$), it is possible to define a reference potential E^{tot}, given by

$$E^{tot} = -\frac{\Delta H^{tot}(T,P)}{2F} \quad (3)$$

In standard conditions, $E^{tot} = 1.25$ V for vapour water and $E^{tot} = 1.48$ V for liquid water (or 1.47 V at $P = 1$ bar and $T = 353$ K). It represents the (fictive) potential that the fuel cell would reach if the totality of chemical energy were transformed into electricity. Of course, according to the second law of thermodynamic, only the Gibbs enthalpy can be directly transformed into electricity; the ideal open circuit voltage (OCV) E^{th} is

$$E^{th} = -\frac{\Delta G^{tot}(T,P)}{2F} \quad (4)$$

Assuming that hydrogen, oxygen and vapour are ideal gases, the reaction Gibbs enthalpy $\Delta G^{tot}(T,P)$ can be calculated with the following expression:

$$\Delta G^{tot}(T,P) = \Delta G^0 - \int_{298\ K}^{T} \Delta S^{tot}(T,P^0)\cdot dT + RT \ln\left(\frac{a_{H_2O}}{a_{H_2} a_{O_2}^{1/2}}\right) \quad (5)$$

where $a_i = 1$ in liquid phase; $a_i = P^i/P^0$ for gases, with P^i the partial pressure and P^0 the standard pressure. ΔG^0 stands for the Gibbs enthalpy of the reaction in standard conditions and $\Delta S^{tot}(T,P^0)$ stands for the reaction entropy, the gases being at standard pressure. Note that the values of $\Delta H^{tot}(T,P)$, $\Delta G^{tot}(T,P)$ and $\Delta S^{tot}(T,P^0)$ differ according to the state of water (liquid or vapour). If the temperature remains close to 298 K (which is the case with PEMFC), it is possible to consider that $\Delta S^{tot}(T,P^0) \cong \Delta S^0$ and to derive the following expressions for fuel cell thermodynamic potential:

$$E^{th}(T,P) = 1.184 - 0.00023(T - 298) + \frac{RT}{2F} \ln\left(\frac{a_{H_2} a_{O_2}^{1/2}}{a_{H_2O}}\right) \quad (6)$$

$$E^{th}(T,P) = 1.229 - 0.00085(T - 298) + \frac{RT}{2F} \ln(a_{H_2} a_{O_2}^{1/2}) \quad (7)$$

In Eq. (6), it is assumed that water is produced in vapour phase, while it is produced in liquid phase in Eq. (7). Of course, Eqs. (6) and (7) lead to the same result when $P_{H_2O} = P_{sat}$.

The amount of chemical energy that can be converted into electricity is partially dependent on the state of water produced by the

fuel cell (liquid or gas): the difference in enthalpy between saturated vapour and liquid water is heat only but the thermodynamic open circuit voltage $E^{th}(T,P)$ (6) increases (slightly because of the logarithm) if the vapour partial pressure is lower than the saturation pressure. In this paper, water is assumed to be produced in liquid phase in the hydrophilic Nafion of the catalyst layer, which adsorbs and retains liquid water [13].

The real open circuit voltage is lower than $E^{th}(T,P)$. According to the literature, the reasons for this are linked mainly to [14,15]:

- Internal currents and gas cross-over (hydrogen mostly) through the membrane.
- Parasitic half-reactions, like the oxidation of platinum and/or others linked to the presence of impurities, like carbon monoxide.

The various voltage drops in a running fuel cell and their effects on the polarization curve are depicted in Fig. 1 [16]. At low current density, voltage losses are mostly due to the activation of electrochemical reactions. Then, the linear part of the curve is commonly attributed to ohmic losses in the membrane because of its protonic resistance. Finally, at high current density, a sharp fall of the voltage is caused by mass transport limitations (lack of reactive gases at the electrodes and/or flooding). The electrical power lost trough voltage drops is irreversibly degraded into heat, $\dot{Q}_{\Delta V}$.

An additional heat source associated with water condensation/evaporation in the GDLs has to be taken into account, if necessary. In practice, low gas stoichiometry leads to water condensation in the gas channels and/or in the GDLs. The heat released by the water condensation (or consumed in case of evaporation) is not directly linked to the cell voltage. However, when too much liquid water accumulates in the GDL, flooding of the electrode occurs, resulting in critical voltage drop.

3. Localization and quantification of the heat sources

In this section, the localization and the quantification of each type of heat source (or sink) are discussed. From a spatial point of view, three cases can be distinguished (Fig. 2):

- Volumetric sources $\dot{q}_J$, caused by Joule effect due to the protonic resistance of the electrolyte and distributed trough the membrane thickness. The electrical resistance of the GDLs and of the bipolar plates is often neglected because of the high conductivity of these carbonaceous materials.
- Sources that are assumed located at the electrodes:
  - The electrochemical conversion contributes to heat production for two reasons:
    i. Hydrogen oxidation and oxygen reduction are at the origin of a heat source and a heat sink $\dot{Q}^a_{reac}$ and $\dot{Q}^c_{reac}$, respectively, proportional to the entropy of each half-reaction and to the current density.
    ii. Voltage drops at the electrodes due to the activation overpotentials result in heat sources ($\dot{Q}^a_{act}$ and $\dot{Q}^c_{act}$).
  - And heat sources $\dot{Q}^a_{sorp}$ and $\dot{Q}^c_{sorp}$ are associated with water sorption phenomena at the membrane–electrode interfaces.

  Actually, these heat sources are distributed through the volume of the electrodes. Due to their low thickness (about 10 μm compared to the membrane or GDL which have a thickness about 200 μm), they are frequently considered as surface sources. However, it is to be noted that the use of thin membranes like Nafion 112 (50 μm) or Gore membranes (18 μm) makes this hypothesis less tenable.
- Local sources $\dot{q}_{c/e}$ in the GDL related to water phase change (condensation or evaporation), if necessary. These sources can be distributed all over the GDL, depending on mass and heat transfers.

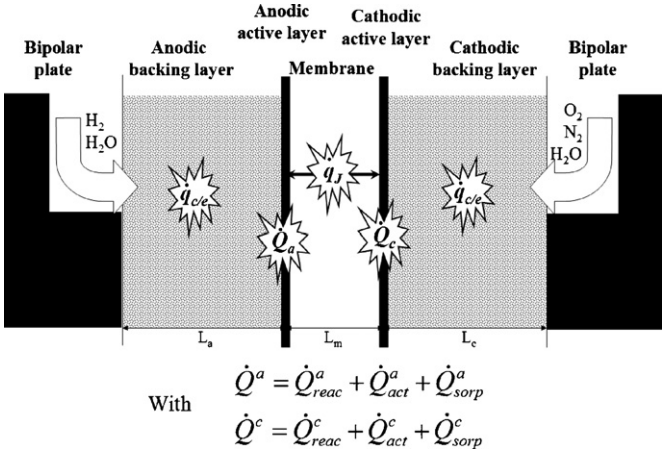

Fig. 2. Heat sources distribution in the cell.

The electrical contact resistances appearing at the interface between the various MEA layers and at the interface between the MEA and the bipolar plates should also be taken into account if they are significant. Experimental measurements of the thermal contact resistances between Toray carbon paper and smooth aluminium bronze versus the compression pressure are given in [17].

3.1. Joule effect

Proton transport from the anode to the cathode through the membrane results in enthalpy variation due to the membrane conductivity:

$$Q_J = 2\Delta H^c_{H^+} - 2\Delta H^a_{H^+} \tag{8}$$

The corresponding voltage loss is then written:

$$V_{ohm} = R_{ohm} i = \frac{Q_J}{2F} \tag{9}$$

The proton transfer resistance R_{ohm} is often estimated after a preliminary study of mass transport giving water distribution in the membrane. Many correlations are proposed in the literature for estimating the local membrane conductivity from its temperature and water content. The most used [18–22] are listed below:

- [18]:

$$\sigma_{H^+}(T) = (0.0013\lambda^3 + 0.0298\lambda^2 + 0.2658\lambda)\exp\left[E_A\left(\frac{1}{303} - \frac{1}{T}\right)\right] \tag{10.1}$$

with $E_A = 2640\exp(-0.6\lambda) + 1183$

- [19]:

$$\sigma_{H^+}(T) = (0.5139\lambda - 0.326)\exp\left[1268\left(\frac{1}{303} - \frac{1}{T}\right)\right] \tag{10.2}$$

- [20]:

$$\sigma_{H^+}(T) = (0.58\lambda - 0.5)\exp\left[1268\left(\frac{1}{303} - \frac{1}{T}\right)\right] \tag{10.3}$$

- [21]:

$$\sigma_{H^+}(T) = (0.46\lambda - 0.25)\exp\left[1190\left(\frac{1}{298.15} - \frac{1}{T}\right)\right] \tag{10.4}$$

- [22]:

$$\begin{aligned} \sigma_{H^+}(T) &= 0 & \lambda &< 1.253 \\ \sigma_{H^+}(T) &= 0.5738\lambda - 0.7192 & \lambda &> 1.253 \end{aligned} \tag{10.5}$$

The total membrane resistance is then obtained by integration of the above local conductivity in the membrane thickness:

$$R_{ohm} = \int_0^{L_m} \frac{1}{\sigma_{H^+}(T,z)} dz \tag{11}$$

Finally, the heat source generated by Joule effect is computed from the membrane resistance R_{ohm}, and the hydrogen molar flux $N_{H_2} = i/2F$:

$$\dot{q}_J = \frac{Q_J}{L_m}\frac{i}{2F} = \frac{R_{ohm} i^2}{L_m} \tag{12}$$

According to this expression, the heat source generated by Joule effect is uniformly distributed in the membrane thickness.

3.2. Heat released by the half-reactions

Even in the case of an ideal fuel cell, there is a minimum part of chemical energy that cannot be directly transformed into work. It corresponds to:

$$Q^{th} = \Delta G^{tot}(T,P) - \Delta H^{tot}(T,P) = -T\Delta S^{tot}_{rev}(T,P) \tag{13}$$

The reversible heat released by the global reaction of hydrogen oxidation (Eq. (1)) is a function of the reaction entropy:

$$\Delta S^{tot}_{rev} = -163.2\,\text{J mol}^{-1}\,\text{K}^{-1} \quad \text{at } T = 353\,\text{K}$$
$$\text{and } P_{H_2} = P_{O_2} = 1\,\text{bar} \tag{14}$$

Taking gas dilution into account leads to the following expression:

$$\Delta S^{tot}_{rev}(T,P) = \Delta S^{tot}_{rev}(T,P^0) - R\ \ln(a_{H_2}\cdot a_{O_2}^{1/2}) \tag{15}$$

The total amount of heat released by the global reaction (in J mol^{-1}) is thus:

$$Q^{tot}_{reac} = -T\Delta S^{tot}_{rev}(T,P) \tag{16}$$

And the corresponding heat flux is:

$$\dot{Q}^{tot}_{reac} = \frac{i}{2F} Q^{tot}_{reac} \tag{17}$$

The expression of Eq. (15) implies that water is produced in liquid phase. If the water partial pressure in the GDL is lower than the saturation pressure, water remains in gas phase and it is necessary to take account of the sorption enthalpy at the cathode.

Although the global reaction entropy is well known, determining which part has to be attributed to each electrode is a less simple task. Indeed, the equations of thermodynamic equilibrium at each electrode (for the half-reactions of hydrogen oxidation and oxygen reduction) use the value of the entropy of the charged species: ΔS_{H^+} and ΔS_{e^-}. These values seem to be roughly known. Actually, it is impossible to make a solution of cations without anions, so that the entropy of ions is not easy to estimate.

A review of the literature highlights this difficulty: as shown in Table 1, the values are widely dispersed. According to the authors, the half-reaction of hydrogen oxidation can be endothermic [25–27] ($Q^a_{reac} < 0$) or exothermic [23,24] ($Q^a_{reac} > 0$). A particular attention should be given to the conditions in which these results were obtained: on the one hand, some authors characterized the whole half-reaction of hydrogen oxidation [23,27] or oxygen reduction [25]. On the other hand, others measured the entropy of hydrogen adsorption on Pt/C electrodes [26].

Table 1
Entropy of the half-reaction of hydrogen oxidation (review).

Entropy of anodic reaction (J mol^{-1} K^{-1})	References
−133.2 ± 2.8	[23]
−42.5	[24]
+0.104	[25]
+69.1	[26]
+84.7 ± 3.5	[27]

However, Bockris and Conway [28] proposed a detailed study of proton solvation in water that helps to estimate the entropy change of the half-reaction of hydrogen oxidation. The anodic process can be written:

$$H_{2gaz} + 2H_2O_{liq} \rightarrow 2H_3O_{liq}{}^+ + 2e^- \tag{18}$$

The overall entropy change can thus be expressed as

$$\Delta S^a_{rev} = 2\Delta S^{sol}_{H_3O^+} + 2\Delta S_{e^-} - \Delta S_{H_{2gaz}} - 2\Delta S_{H_2O_{liq}} \tag{19}$$

where ΔS_{e^-} is the entropy of the electron at the Fermi level. From Sommerfeld's treatment of the Fermi–Dirac statistics, this is known to be equal to the electronic contribution to the specific heat of metals. It is about 0.25 J mol^{-1} K^{-1}, which is far less than the degree of error in the other quantities. It may therefore be neglected.

The common values of gaseous dihydrogen and liquid water entropy are, respectively, $\Delta S_{H_{2gaz}} = +130.6\,\text{J mol}^{-1}\,\text{K}^{-1}$ and $\Delta S_{H_2O_{liq}} = +69.9\,\text{J mol}^{-1}\,\text{K}^{-1}$ [29]. The entropy of solvation of H_3O^+ in water is estimated from its Gibbs enthalpy of solvation, using the Born charging equation [29]:

$$\Delta G^{sol}_{H_3O^+} = -\frac{(ze)^2 N_A}{8\pi\varepsilon_0 r_{eff}}\left(1 - \frac{1}{\varepsilon_r}\right) \tag{20}$$

$\Delta G^{sol}_{H_3O^+}$ is the gain in free energy resulting from importing an electronic charge by integration from infinity ($\varepsilon = 1$) into a medium of dielectric constant ε. In our case $z = 1$; e is the electronic charge, and N_A is the Avogadro's number. Using the standard thermodynamic relationship (Eq. (21)) and the Abegg's empirical equation for the dielectric constant (Eqs. (22) and (20)) leads to the following analytical expressions for the enthalpy and the entropy of H_3O^+ solvation (Eqs. (23) and (24), respectively),

$$\Delta H^{sol}_{H_3O^+} = \Delta G^{sol}_{H_3O^+} - T\left(\frac{d\Delta G^{sol}_{H_3O^+}}{dT}\right)_P \tag{21}$$

$$\varepsilon_r = \varepsilon_r(T=0)\cdot\exp(-TL) \tag{22}$$

where the Abegg's constant is set to $L = 4.8 \times 10{-}3\,\text{K}^{-1}$ [29].

$$\Delta H^{sol}_{H_3O^+} = -\frac{(ze)^2 N_A}{8\pi\varepsilon_0\varepsilon_r r_{eff}}\left[1 - \left(1 - \frac{TL}{\varepsilon_r}\right)\right] \tag{23}$$

$$\Delta S^{sol}_{H_3O^+} = \frac{(ze)^2 N_A}{8\pi\varepsilon_0\varepsilon_r r_{eff}} \tag{24}$$

According to Conway studies [28], the enthalpy of H_3O^+ solvation is $\Delta H^{sol}_{H_3O^+} = -381\,\text{kJ mol}^{-1}$. This value is fitted via Eq. (23) to give an effective ionic radius r_{eff} of 1.82 Å. Using this value in Eq. (24), we obtain $\Delta S^{sol}_{H_3O^+} = +22.2\,\text{J mol}^{-1}\,\text{K}^{-1}$.

Finally, the overall anodic entropy change is estimated according to Eq. (19):

$$\Delta S^a_{rev} = -226\,\text{J mol}^{-1}\,\text{K}^{-1} \tag{25}$$

According to this analysis, the anodic reaction is highly exothermic. The cathodic reaction entropy change is then deduced from the undisputable entropy change of the overall reaction (Eq. (14)):

$$\Delta S^c_{rev} = \Delta S^{tot}_{rev} - \Delta S^a_{rev} = +62.8\,\text{J mol}^{-1}\,\text{K}^{-1} \tag{26}$$

The cathodic process is therefore endothermic.

Because of the lack of reliable data, many authors consider the anodic half-reaction as isothermal ($Q^a_{reac} = 0$) [3,30] and consequently, the entropy of water formation reaction is fully attributed

to the oxygen reduction, leading to an exothermic cathodic half-reaction. This assumption, commonly used in the literature is in contradiction with the above analysis.

The heat fluxes generated under reversible conditions by the half-reactions are given by

$$\dot{Q}^i_{reac} = Q^i_{reac}\frac{i}{2F} \tag{27}$$

3.3. Electrochemical activation of reactions

According to the activated complex theory, the electrochemical reactions are responsible for a part of the energy degradation.

$$Q^a_{act} = -T\Delta S^a_{irr}(T,P) \quad \text{and} \quad Q^c_{act} = -T\Delta S^c_{irr}(T,P) \tag{28}$$

These irreversibilities result in overpotentials at the electrodes, depending on current density, geometrical parameters and reactants properties (temperature, pressure and concentration).

$$\eta^a = -\frac{Q^a_{act}}{2F} \quad \text{and} \quad \eta^c = -\frac{Q^c_{act}}{2F} \tag{29}$$

Although the anodic and cathodic overpotentials η^a and η^c are often calculated from a Tafel equation, they can be estimated thanks to any model of mass and charge transfer in the electrodes [7,31–34].

Knowing the overpotentials, the heat flux generated by the activation of the electrochemical reactions is given by

$$\dot{Q}^a_{act} = -Q^a_{act}\frac{i}{2F} = \eta^a i \quad \text{and} \quad \dot{Q}^c_{act} = -Q^c_{act}\frac{i}{2F} = \eta^c i \tag{30}$$

3.4. Sorption/desorption

Since water is assumed to be produced in liquid phase, sorption/desorption of the water must be taken into account at the electrodes. The sorption phenomenon is governed by the balance between a liquid phase (adsorbed) and a gaseous phase (desorbed) at an interface. Water in fuel cells is subjected to sorption at the interfaces between membrane, where water is in liquid phase and the GDLs, where water is mainly vapour. The sorption enthalpy ΔH_{sorp} is

$$\Delta H_{sorp} = \Delta H^f_{H_2O_{ad}} - \Delta H^f_{H_2O_{gas}} \tag{31}$$

In [35], the authors observed that the sorption enthalpy of water in Nafion 117 varies with the membrane hydration and that it is dependent on pre-treatment. However, no general trends can be drawn. Watari et al. [36] present a review of the values proposed in the literature. They also measured values decreasing from 52 to 45 kJ mol^{-1} in the case of sulfonated polyimide membranes. More recently, Burnett et al. [37] experimented with Nafion 112 and found values pretty close to the latent heat of water. All these results are listed in Table 2.

Since most of the values encountered in the literature are close to the latent heat of water (L_v = 41.6 kJ mol^{-1} at 353 K [29]), the sorption enthalpy of water is often assumed equal to L_v.

The heat released (or consumed) by this change of phase is a function of the water flux subjected to sorption/desorption and of the sorption enthalpy ΔH_{sorp}. The water flux at the membrane/GDLs interfaces can be estimated according to any description of mass transport in the membrane electrode assembly (MEA). This flux is perpendicular to the membrane and counted algebraically, which makes it possible to treat sorption and desorption in the same way.

$$\dot{Q}^a_{sorp} = \Delta H_{sorp} N^a_{H_2O} \quad \text{and} \quad \dot{Q}^c_{sorp} = -\Delta H_{sorp} N^c_{H_2O} \tag{32}$$

with $N^c_{H_2O} = N^a_{H_2O} + i/2F$ to take into account of the water produced in liquid phase at the cathode. Note that in some particular cases, the water adsorption and desorption in the membrane can generate important heat source and sink at the electrodes (for instance when one side of the membrane is in contact with dry hydrogen while the other is in contact with humidified air). This phenomenon is neglected in most of the thermal studies.

Table 2
Water sorption enthalpy in membranes (review).

Enthalpy sorption (kJ mol^{-1})	Reference	Comments
46	[38]	For Nafion 112 For $a_w > 0.2$
From 60 to 43	[37]	For Nafion 112 Decreasing with increasing water uptake
From 52.3 to 16.7	[39]	For Nafion 117 For $a_w > 0.2$ Decreasing with increasing water uptake
28	[40]	For Nafion 117 For $a_w > 0.2$
From 45 to 110	[35]	For Nafion 117 A function of water uptake and Nafion pretreatement
45	[36]	For Nafion 117
43	[41]	For non-sulfonated polyimide membranes
From 52 to 45	[36]	For sulfonated polyimide membranes Decreasing with an increasing water uptake

3.5. Water condensation/evaporation

Water condensation occurs when the partial pressure of vapour reaches the saturation pressure. This saturation pressure depends strongly on temperature as shown by Antoine's equation with the following coefficients:

$$P_{sat} = P^0 \exp\left(13.669 - \frac{5096.23}{T}\right) \tag{33}$$

In order to determine the condensation sites, the vapour pressure profiles have to be compared to the fields of vapour saturation pressure deduced from temperatures. Due to water production at the cathode, vapour partial pressures are slightly higher nearby the membrane and lower at the bipolar plates/GDL interface. However, according to the results presented in [42], the vapour pressure gradients in the GDL are lower than the vapour saturation pressure gradients resulting from temperature distribution, even with a high GDL thermal conductivity. This means that condensation will occur preferentially at the cold spots of the cell (i.e. at the ribs of the bipolar plates), where the saturation pressure is the lowest, although the cathode remains the place where the vapour partial pressure is the highest. This observation is confirmed by the fully coupled model of heat and mass transfers presented by Weber and Newman [43] but it is in contradiction with conclusions issued from isothermal mass transfer models, where condensation could only occur at the cathode. This remark highlights the importance of accurate thermal and mass coupled modeling to determine the condensation sites in the cell. To confirm these remarks, a complete modeling of coupled heat, charge and mass transfers has to be carried out in a bi-dimensional (or three-dimensional) geometry.

Once the condensation sites identified, the associated heat source is easily computed from the latent heat of water $L_v = (T)$ at the temperature T:

$$L_v(T^0) = \Delta H^f_{H_2O_{liq}} - \Delta H^f_{H_2O_{vap}} \tag{34}$$

At 353 K, L_v = 41.6 kJ mol^{-1} [29].

Let us denote $n_{vap\rightarrow liq}$ the water quantity to be condensed. $n_{vap\rightarrow liq}$ is positive when condensation occurs, and negative in case

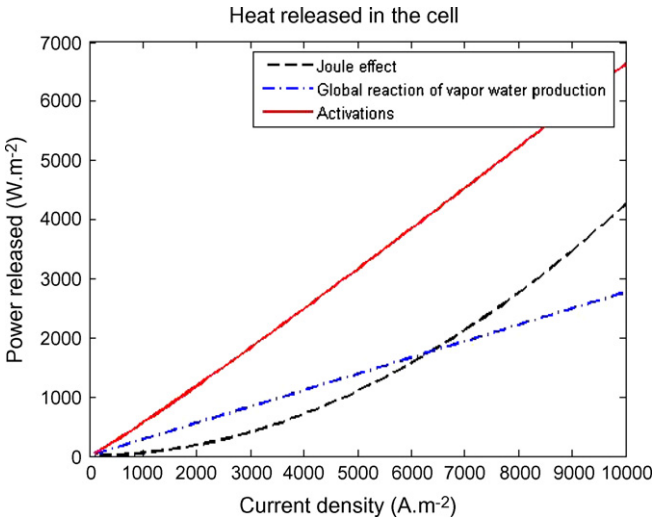

Fig. 3. Heat sources as functions of current density.

of evaporation. The local heat source associated to water condensation/evaporation is given by

$$\dot{q}_{c/e} = n_{vap\rightarrow liq} L_v \tag{35}$$

The same expression is valid for both evaporation and condensation, since $n_{vap\rightarrow liq}$ is counted algebraically.

4. Heat sources variation with the current density

$RH^a = RH^c = 0.90$

$T_{water} = T_{H_2} = T_{Air} = 353\,\mathrm{K}$

Fig. 3 depicts the relative importance of heat sources (by reference to the membrane surface: $\dot{Q}_J = \dot{q}_J L_m$), as functions of the current density. It is assumed that no water condensation occurs within the fuel cell. The membrane resistance R_{ohm} is set to $4.4 \times 10^{-5}\,\Omega\,m^2$, which can be considered as the worst case, corresponding for instance to a 125 μm-thick membrane humidified only by vapour (without liquid water on the electrodes) (Eq. (11)). Actual values of membrane resistance currently reported in the literature can be about three times lower [44]. The activation overpotentials are estimated thanks to a Tafel law. The aim of Fig. 3 is only to compare the relative magnitude of heat sources of various origins. A detailed model of heat and mass transfer is needed for the proper evaluation of the local heat sources/sinks in the cell, as functions of local concentration and water fluxes; this is out of the scope of this paper. Unfortunately, this representation conceals the effects of local heat sinks.

The heat source associated with the global reaction of hydrogen oxidation is calculated as follows:

$$\dot{Q}^{tot}_{reac} = \dot{Q}^{a}_{reac} + \dot{Q}^{c}_{reac} - \frac{i}{2F}\Delta H_{sorp} \tag{36}$$

with $\Delta H_{sorp} = L_v$. $\dot{Q}^{a}_{reac}$ and $\dot{Q}^{c}_{reac}$ are the anodic and cathodic reversible heat sources related to the electrochemical half-reactions, respectively. The last term in the right hand side of (Eq. (36)) stands for the sum of sorption/desorption contributions at the electrodes (Eq. (32)). The result of (Eq. (36)) is consequently nearly independent from mass transport in the membrane. The activation overpotentials depend slightly on hydrogen and oxygen concentration at the electrodes. Only the Joule effect in the membrane depends significantly on its water content.

Fig. 3 shows that the activation overpotentials are the highest heat sources. The global reaction of hydrogen oxidation $\dot{Q}^{tot}_{reac}$ cannot be neglected: it is the lowest heat source in the present example but it is expected to be more significant than the Joule effect in a fuel cell using a thinner membrane. These results are in good agreement with those presented by Ju et al. [10].

As detailed previously, although the whole reaction results in heat production, the cathodic half-reaction is endothermic and the anodic one is exothermic. Thereby, this analysis is in contradiction with the assumption commonly found in the literature of an exothermic cathodic reaction (and isothermal anodic half-reaction). In the same way, water desorption heat sink is partly counterbalanced by the water sorption heat source. However, one can imagine that in the case of large water flux through the membrane, water sorption/desorption would result in a large heat sink at one electrode and a large heat source at the other one.

5. Conclusions

The global heat flux generated by a fuel cell is directly dependent on its electrical performances and is therefore easy to estimate. However, an accurate review of all heat sources within the MEA put forward some difficulties in estimating local heat sources/sinks, which results in bold assumptions commonly encountered in the literature.

First, because of a lack of pertinent thermodynamical study on both half-reactions, most of the authors assume that the anodic half-reaction is isothermal and that consequently, the entropy of water formation reaction is fully attributed to the oxygen reduction, leading to an exothermic half-reaction ($\Delta S^{tot}_{rev} = -163.2\,\mathrm{J\,mol^{-1}\,K^{-1}}$). The analysis presented in this paper rather suggests that the oxygen reduction reaction is endothermic ($\Delta S^{c}_{rev} = +62.8\,\mathrm{J\,mol^{-1}\,K^{-1}}$), whereas the hydrogen oxidation reaction is highly exothermic ($\Delta S^{a}_{rev} = -226\,\mathrm{J\,mol^{-1}\,K^{-1}}$). As a consequence, thermal gradients in the different layers of the MEA (membrane, GDL, etc.) are probably larger than routinely thought.

The thermal description also necessitates to take account of water sorption/desorption phenomena at the electrodes: heat sinks or sources can appear, depending on the direction and intensity of the water flux through the membrane.

Finally, the water phase change can result in local heat sources/sinks in the GDL also. Since the water saturation pressure is a function of temperature (Eq. (33)), water phase change is governed by both thermal and water distributions in the GDL. A fully coupled model of heat and mass transfers is thus needed to identify the place of water condensation and evaporation.

As a conclusion, it seems that most of the thermal transfer studies tend to oversimplify the models. The global heat source is generally well identified, but badly apportioned. As a consequence, heat sinks are almost always neglected and thermal gradients, in particular in the membrane, may be larger than expected.

References

[1] D. Hyun, J. Kim, Study of external humidification method in proton exchange membrane fuel cell, J. Power Sources 126 (2004) 98–103.
[2] W.-M. Yan, F. Chen, H.-Y. Wu, C.-Y. Soong, H.-S. Chu, Analysis of thermal and water management with temperature-dependent diffusion effects in membrane of proton exchange membrane fuel cells, J. Power Sources 129 (2004) 127–137.
[3] H. Wu, P. Berg, X. Li, Non-isothermal transient modeling of water transport in PEM fuel cells, J. Power Sources 165 (2007) 232–243.
[4] A. Faghri, Z. Guo, Challenges and opportunities of thermal management issues related to fuel cell technology and modeling, Int. J. Heat Mass Transfer 48 (2005) 3891–3920.
[5] C.-Y. Wang, Fundamental models for fuel cell engineering, Chem. Rev. 104 (2004) 4727–47666.
[6] T.F. Fueller, J. Newman, Water and thermal management in solid–polymer–electrolyte fuel cells, J. Electrochem. Soc. 140 (1993) 1218–1225.
[7] J. Ramousse, J. Deseure, S. Didierjean, O. Lottin, D. Maillet, Modeling of heat, mass and charge transfers in a PEMFC single cell, J. Power Sources 145 (2005) 416–427.

[8] A. Rowe, X. Li, Mathematical modeling of proton exchange membrane fuel cells, J. Power Sources 102 (2001) 82–96.
[9] N. Djilali, D. Lu, Influence of heat transfer on gas and water transport in fuel cells, Int. J. Therm. Sci. 41 (2002) 29–40.
[10] H. Ju, H. Meng, C.-Y. Wang, A single-phase, non isothermal model for PEM fuel cells, Int. J. Heat Mass Transfer 48 (2005) 1303–1315.
[11] G.F. Naterer, C.D. Tokarz, J. Avsec, Fuel cell entropy production with ohmic heating and diffusive polarization, Int. J. Heat Mass Transfer 49 (2006) 2673–2683.
[12] S. Kjelstrup, A. Rosjorde, Local and total entropy production and heat and water fluxes in a one-dimensional polymer electrolyte fuel cell, J. Phys. Chem. B 109 (2005) 9020–9033.
[13] M. Laporta, M. Pegoraro, L. Zanderighi, Perfluorosulfonated membrane (Nafion): FT-IR study of the state of water with increasing humidity, Phys. Chem. Chem. Phys. 1 (1999) 4619–4628.
[14] X. Zhu, H. Zhang, Y. Zhang, Y. Liang, X. Wang, B. Yi, An ultrathin self-humidified membrane for PEM fuel cell application: fabrication, characterization and experimental analysis, J. Phys. Chem. 110 (2006) 14240–14248.
[15] J. Zhang, Y. Tang, C. Song, J. Zhang, H. Wang, PEM fuel cell open circuit voltage (OCV) in the temperature range of 23 °C to 120 °C, J. Power Sources 163 (2006) 532–537.
[16] J. Larminie, A. Dicks, Fuel Cell Systems Explained, Wiley Editions, New York, 2000.
[17] M. Khandelwal, M.M. Mench, Direct measurement of through-plane thermal conductivity and contact resistance in fuel cell materials, J. Power Sources 161 (2006) 1106–1115.
[18] W. Neubrand, Modelbildung und Simulation von Elektromembranverfahren, PhD Thesis, 1999.
[19] T.E. Springer, T.A. Zawodzinski, S. Gottesfeld, Polymer electrolyte fuel cell model, J. Electrochem. Soc. 138 (1991) 2334–2342.
[20] P. Costamagna, Transport phenomena in polymeric membrane fuel cells, Chem. Eng. Sci. 56 (2001) 67–74.
[21] F. Meier, G. Eigenberger, Transport parameters for the modelling of water transport in ionomer membranes for PEMFC fuel cells, Electrochim. Acta 49 (2004) 1731–1742.
[22] A.A. Kulikovsky, Quasi-3D modeling of water transport in polymer electrolyte fuel cells, J. Electrochem. Soc. 150 (2003) A1432–A1439.
[23] A.L. Rockwood, Absolute half-cell entropy, Phys. Rev. A 36 (1987) 1525–1526.
[24] N.P. Siegel, M.W. Ellis, D.J. Nelson, M.R. von, Spakovsky, A two-dimensional computational model of a PEMFC with liquid water transport, J. Power Sources 128 (2004) 173–184.
[25] M. Lampinen, M. Fomino, Analysis of free energy and entropy changes for half-cell reactions, J. Electrochem. Soc. 140 (1993) 3537–3546.
[26] N.R. Elezovic, B.M. Babic, N.V. Krstajic, L.M. Gajic-Krstajic, Lj.M. Vracar, Specificity of the UPD of H to the structure of highly dispersed Pt on carbon support, Int. J. Hydrogen Energy 32 (2006) 1991–1998.
[27] B.E. Conway, D.P. Wilkinson, Non-isothermal cell potentials and evaluation of entropies of ions and of activation for single electrode processes in non-aqueous media, Electrochim. Acta 38 (1993) 997–1013.
[28] J.O'M. Bockris, B.E. Conway, Modern Aspects of Electrochemistry, vol. 3, Butterworth Editions, London, 1964.
[29] P. Atkins, J. de Paula, Physical Chemistry, 7th edition, Oxford University Press, 2002.
[30] S. Kjelstrup, A. Rosjorde, Local Entropy Production, Heat and Water Fluxes Out of a One-dimensional Polymer Electrolyte Fuel Cell, ECOS, Copenhagen, Denmark, 2003.
[31] T.E. Springer, I.D. Raistrick, Electrical impedance of a wall for the flooded-agglomerate model of porous gas diffusion electrodes, J. Electrochem. Soc. 136 (1989) 1594–1603.
[32] M. Eikerling, A.A. Kornyshev, Modelling the performance of the cathode catalyst layer of polymer electrolyte fuel cells, J. Electroanal. Chem. 475 (1999) 107–123.
[33] F. Gloaguen, P. Convert, S. Gamburzev, O.A. Velev, S. Srinivasan, An evaluation of the macro-homogenous and agglomerate model for oxygen reduction in PEMFCs, Electrochim. Acta 43–24 (1998) 3767–3772.
[34] Y. Bultel, L. Genies, O. Antoine, P. Ozil, R. Durand, Modeling impedance diagrams of active layers in gas diffusion electrodes: diffusion, ohmic drop effects and multistep reactions, J. Electroanal. Chem. 527 (2002) 143–155.
[35] P.J. Reucroft, D. Rivin, N.S. Schneider, Thermodynamics of Nafion™–vapor interactions. I. Water vapor, Polymer 43 (2002) 5157–5161.
[36] T. Watari, H. Wang, K. Kuwahara, K. Tanaka, H. Kita, K. Okamoto, Water vapor sorption and diffusion properties of sulfonated polyimide membranes, J. Membr. Sci. 219 (2003) 137–147.
[37] D.J. Burnett, A.R. Garcia, F. Thielmann, Measuring moisture sorption and diffusion kinetics on proton exchange membranes using a gravimetric vapor sorption apparatus, J. Power Sources 160 (2006) 426–430.
[38] K. Mizoguchi, K. Terada, Y. Naito, Y. Kamiya, Gas transport in Nafion membrane, Polym. Prep. 49 (2000) 3517–3518.
[39] M. Escoubes, M. Pineri, Perfluorinated Ionomer Membranes, ACS Symposium Series No. 180, Washington, DC, USA, 1982.
[40] D.R. Morris, X. Sun, Water sorption and transport properties of Nafion 117, J. Appl. Polym. Sci. 50 (1993) 1445–1452.
[41] K. Okamoto, Sorption and diffusion of water vapor in polyimide films, in: M.K. Ghosh, K.L. Mittal (Eds.), Polyimides Fundamentals and Applications, Marcel Dekker, New York, USA, 1996, pp. 265–278.
[42] J. Ramousse, S. Didierjean, O. Lottin, D. Maillet, Thermal Fields and Saturation Discussion in a PEMFC Single Cell, HFC, Vancouver, Canada, 2007.
[43] A.Z. Weber, J. Newman, Coupled thermal and water management in polymer–electrolyte fuel cells, J. Electrochem. Soc. 153 (2006) A2205–A2214.
[44] J. Mainka, G. Maranzana, J. Dillet, S. Didierjean, O. Lottin, Investigation on the Origin of Diffusion Impedance in The Porous Cathode of a Proton Exchange Membrane Fuel Cell (PEMFC) Via Electrochemical Impedance Spectroscopy (EIS), FDFC08, Nancy, France, 2008.